Size Evolution of Alkanethiol-Protected Gold Nanoparticles by Heat Treatment in the Solid State

Takami Shimizu,[†] Toshiharu Teranishi,[†,‡] Satoshi Hasegawa,[†] and Mikio Miyake*[,†]

School of Materials Science, Japan Advanced Institute of Science and Technology, and Organization and Function, PRESTO, Japan Science and Technology Corporation, 1-1 Asahidai, Tatsunokuchi, Nomi, Ishikawa 923-1292, Japan

Received: September 6, 2002; In Final Form: January 7, 2003

A simple method is proposed to control the size of alkanethiol-protected Au nanoparticles by heat treatment in the solid state. The mean diameter of the Au nanoparticles prepared by Brust's two-phase method (∼1.5 nm) was evolved to 3.4−9.7 nm by heating to 150−250 °C in air. The uniform growth of nanoparticles was not observed when tetraoctylammonium bromide (TOAB), which was used as a phase-transfer agent during the preparation of Au nanoparticles, was removed before the particle growth process. The crystal structures of Au nanoparticles and alkanethiol ligand structures on Au nanoparticles were characterized before and after the heat treatment. The size-evolution mechanism was discussed on the basis of the thermodynamic model. The heat-treated Au nanoparticles easily formed self-assembled 2D superlattices with hexagonal packing, where the alkanethiol protective agents with an all-trans conformation were estimated to interpenetrate each other.

Introduction

Much attention has been paid to metal nanoparticles because of their potential use as advanced materials with new electronic and magnetic devices and optical properties.[1−5] However, superlattices of metal nanoparticles are expected to show novel properties that are not present in the isolated particles.[6] The 1D[7] and 2D superlattices[8−12] of Au nanoparticles smaller than 2 nm would be applied to the single-electron tunneling devices using Coulomb blockade phenomenon at room temperature, whereas 2D and 3D superlattices of larger particles would be applied to optical devices such as nonlinear optical devices.[13] Precise control of particle size is very important not only for fabricating the perfect superlattices of Au nanoparticles but also for investigating their size-dependent physical and chemical properties.

Various chemical methods have been developed to control the size of metal nanoparticles just by changing the preparative conditions such as the kind and/or the amount of protective agents.[14−18] However, one disadvantage to these methods is that the nanoparticles should be prepared at low metal concentration, resulting in a low yield of solid samples. In 1994, a noteworthy preparative technique of alkanethiol-protected Au nanoparticles using a two-phase (toluene/water) reaction with a phase-transfer catalyst was reported by Brust and co-workers.[19,20] The important point to note is that small (∼2 nm) monodispersed Au nanoparticles are obtained at very high Au concentration in solution (i.e., a large number of these nanoparticles are available as a solid by evaporating the nanoparticle solution). Then, Leff and co-workers modified this technique to control the particle size by changing the Au/alkanethiol molar ratios, but the size distribution was slightly wide.[21] Recently, Maye and co-workers reported the size and shape manipulation of alkanethiol-protected Au nanoparticles by heat treatment in solution.[22,23] Although such a heat treatment of Au nanoparticles in solution gave larger particles with quite a narrow size distribution, it includes a restriction that originates from preparative conditions in solution such as the solubility of nanoparticles or the boiling point of the solvent.

To control the particle size over a wider range and further the convenient mass production of Au nanoparticles, a size-control procedure in the solid state is favorable.[24] Here, we report a simple heat-treatment method to manipulate the size of Au nanoparticles in the solid state. Au nanoparticles with precisely controlled sizes between 3 and 10 nm are prepared at heat-treatment temperature between 150 and 250 °C. The size-evolution mechanism is discussed on the basis of the thermodynamic model. These size-controlled Au nanoparticles easily form self-assembled 2D superlattices on the flat carbon substrates. The structures of alkanethiol protective agents before and after the heat treatment were characterized in relation to the formation of 2D superlattices.

Experimental Section

Materials. The following chemicals were used as purchased: dodecanethiol (DT), hydrogen tetrachloroaurate (III) tetrahydrate ($HAuCl_4 \cdot 4H_2O$), tetraoctylammonium bromide (TOAB), sodium borohydride ($NaBH_4$) from Wako Chemicals, and octadecanethiol (ODT) from Tokyo Kasei Kogyo. Toluene and methanol were guaranteed grade and were used without further purification.

Synthetic Procedure of Alkanethiol-Protected Au Nanoparticles. A preparation of dodecanethiol-protected Au (DT−Au) nanoparticles as a source for the heat treatment followed the Brust's two-phase reaction procedure.[19] The $HAuCl_4 \cdot 4H_2O$ (0.6 mmol) aqueous solution (60 mL) was added to TOAB (1.2 mmol) in toluene (160 mL), and the mixture was vigorously stirred. The yellow aqueous solution became colorless, and the toluene phase turned orange as a result of the transformation of $[AuCl_4]^-$ with tetraoctylammonium cations. After stirring the

* Corresponding author. E-mail: miyake@jaist.ac.jp.
† Japan Advanced Institute of Science and Technology.
‡ PRESTO, Japan Science and Technology Corporation.

10.1021/jp026920g CCC: $25.00 © 2003 American Chemical Society
Published on Web 03/05/2003

solution mixed with dodecanethiol (0.6 mmol) in toluene (20 mL) for 10 min at room temperature, a freshly prepared aqueous solution (60 mL) of sodium borohydride (6 mmol) was added to the vigorously stirred solution. The resulting solution immediately turned from orange to deep brown and continued to be stirred for more than 12 h. The organic phase was then separated, evaporated in a rotary evaporator at 40 °C, and dried in vacuo at 30 °C for 1 day. Octadecanethiol (ODT) was also used as a protective agent in place of dodecanethiol.

The crude solid that was obtained was heat treated at a prescribed temperature of 150−250 °C with the heating rate of 2 °C min^{-1} and was held for 30 min in air. The heat-treated product was dissolved in 30 mL of toluene and mixed with 300 mL of methanol to remove excess alkanethiol and TOAB. The dark-brown precipitate was filtered off, washed with methanol, and redispersed in toluene. The purified products were confirmed by XPS measurements to be free from TOAB and excess alkanethiol (i.e., no peaks originating from N 1s (401.5 eV), Br $3d_{5/2}$ (67.5 eV), and S $2p_{3/2}$ (167.8 eV) were observed).

Characterization. The consumption of $[AuCl_4]^-$ ions and the formation of DT−Au nanoparticles were confirmed by UV−vis spectroscopy with a Hitachi U-3310 UV−vis spectrophotometer. The weight ratios of Au and DT of DT−Au nanoparticles before and after heat treatment were estimated by thermogravimetric analysis (TGA) on a ULVAC-RIKO TGD9700 from room temperature to 600 °C with a heating rate of 2 °C min^{-1} and were held at 600 °C for 30 min. The elemental composition of DT present on Au nanoparticles before and after heat treatment at various temperatures was estimated by using an elementar Vario EL III. Fourier transform infrared (FT-IR) spectroscopy (HORIBA FT-720) was applied to investigate the conformation of the DT ligands on Au nanoparticles in the solid state by a KBr method.

The alkanethiol-protected Au nanoparticles were observed by transmission electron microscopy (TEM) at 125 kV on a Hitachi H-7100. The specimens for TEM were prepared by placing a few drops of a toluene solution of Au nanoparticles onto the flat amorphous carbon-coated copper grids. The mean diameters and standard deviations of Au nanoparticles were calculated by counting 200 particles with a loupe from TEM images of 400 000× magnification. The crystal structure of the DT−Au nanoparticles was determined by both high-resolution TEM (HRTEM) at 300 kV on a Hitachi H-9000NAR and X-ray powder diffraction (XRD) on a MAC Science M18XHF-SRA with Cu Kα radiation. Atomic force microscopy (AFM) measurements were carried out with a Digital Instruments Nanoscope III with a multimode head. Tapping mode was employed in this study by using NANOSENSORS silicon tips. The Au nanoparticle specimens for AFM were prepared by evaporating a few drops of toluene solution containing DT−Au nanoparticles on mica and highly oriented pyrolytic graphite (HOPG).

Results and Discussion

Heat-Induced Size Evolution of Au Nanoparticles in the Solid State. The toluene solution containing $[AuCl_4]^-$ before reduction shows a peak at 350 nm in its UV−vis spectrum due to the ligand-to-metal charge-transfer transition of the $[AuCl_4]^-$ ions, as shown in Figure 1a. After the reduction of $[AuCl_4]^-$ with sodium borohydride, the solution changed from orange to deep brown, and very weak surface plasmon absorption appeared at around 520 nm (Figure 1b), suggesting the formation of quite small particles.[25] This was confirmed by TEM observation (i.e., as-prepared DT−Au nanoparticles had a mean diameter of 1.5 nm with a standard deviation of 0.2 nm (see Figure 2a)). The mean diameter of as-prepared octadecanethiol-protected Au (ODT−Au) nanoparticles is also 1.5 nm. These small nanoparticles do not form 2D superlattices on a flat carbon-coated copper grid probably because of weak van der Waals attractive forces between the Au nanoparticles. Using a ligand with functional groups to induce the interaction between the ligands has a large effect on the ordering of Au nanoparticles smaller than 2 nm.[12]

To evolve the size of DT−Au nanoparticles, the crude solid prepared by evaporating toluene from a 1.5-nm DT−Au

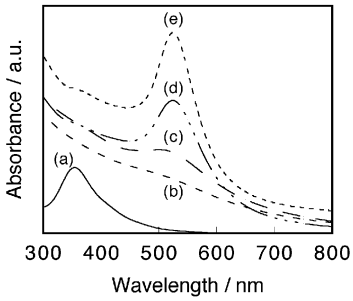

Figure 1. UV−vis spectra of solutions (a) containing $[AuCl_4]^-$ before reduction and (b) immediately after reduction and DT−Au nanoparticles after heat treatment at (c) 150, (d) 190, and (e) 230 °C.

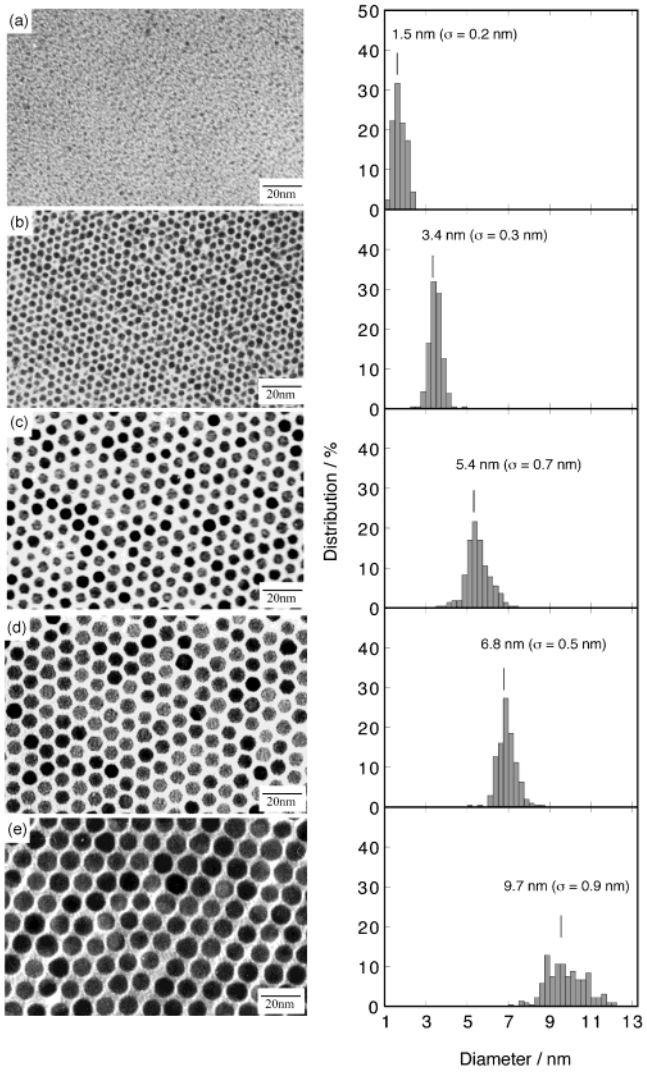

Figure 2. TEM images and size distributions of DT−Au nanoparticles (a) as-prepared and after heat treatment at (b) 150, (c) 190, and (d) 230 °C and (e) ODT−Au nanoparticles heat treated at 250 °C.

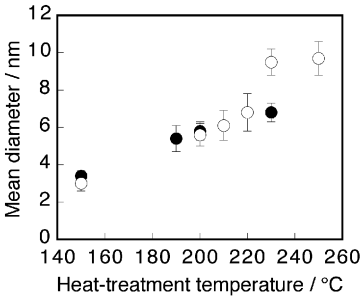

Figure 3. Temperature dependence of the sizes of DT−Au nanoparticles (●) and ODT−Au nanoparticles (○).

nanoparticle solution was heat treated. The TEM images and size distributions of the DT−Au nanoparticles after the heat treatments at 150, 190, and 230 °C are shown in Figure 2b, c, and d, respectively. The size of DT−Au nanoparticles clearly grew by increasing the heat-treatment temperature, the particle sizes being 3.4 ± 0.3, 5.4 ± 0.7, and 6.8 ± 0.5 nm at 150, 190, and 230 °C, respectively. The UV−vis spectra of the toluene solution of heat-treated DT−Au nanoparticles are shown in Figure 1c, d, and e. The intensity of the absorption peak at around 520 nm originated from surface plasmon increases with an increase in the particle size, accompanied by a decrease in the peak width. Such observed features coincide with the prediction of the Mie thoery.[25] For the heat-treatment process, TOAB, adopted as phase-transfer agent during the preparation of DT−Au nanoparticles, plays a key role because the uniform growth of nanoparticles was not observed without TOAB molecules. Presumably, molten TOAB serves as a solvent in the particle growth process. When the DT−Au nanoparticles were heat treated at 250 °C, they were not redispersed in toluene because of the aggregation. This might result from the vaporization of DT ligands because the heat-treatment temperature of 250 °C is very close to the boiling point of DT.

To obtain the larger particles, ODT, having a higher boiling point (204−210 °C/11 mmHg) than DT, was used as a protective ligand in place of DT. At the heat-treatment temperature of 250 °C, ODT−Au nanoparticles grew to 9.7 ± 0.9 nm, as observed from TEM images shown in Figure 2e. The relationship between the mean diameters of the heat-treated DT− and ODT−Au nanoparticles and the heat-treatment temperatures are summarized in Figure 3. Once the small nanoparticles were prepared, we could easily obtain the monodispersed Au nanoparticles from 3.4 to 9.7 nm in size depending on the heat-treatment temperature from 150 to 250 °C.

Crystal Structure of Size-Evolved Au Nanoparticles. The crystal structure of heat-treated DT−Au nanoparticles was investigated by HRTEM and XRD. In a HRTEM image of DT−Au nanoparticles heat-induced at 150 °C (Figure 4), all DT−Au nanoparticles show lattice images originating from a single crystal. The lattice spacing of 0.24 nm is in good agreement with that of the bulk Au{111} plane (0.2355 nm). Since the lattice planes of each particle are randomly arranged, the brightness of the nanoparticles varies in low-magnification TEM images in Figure 2. XRD patterns of the DT−Au nanoparticles with mean diameters of 3.4, 5.4, and 6.8 nm are shown in Figure 5. Several peaks were observed in every XRD pattern at 38.1, 44.4, 64.8, 77.8, and 82.2°, which correspond to the {111}, {200}, {220}, {311}, and {222} planes of the face-centered cubic structure of bulk Au, respectively. Their half-width became narrower for larger particles, whereas the lattice constant remained unchanged. The interplane spacing of the {111} plane calculated from the diffraction angle of 38.1° is 0.236 nm, in good agreement with that of the bulk Au{111} plane.

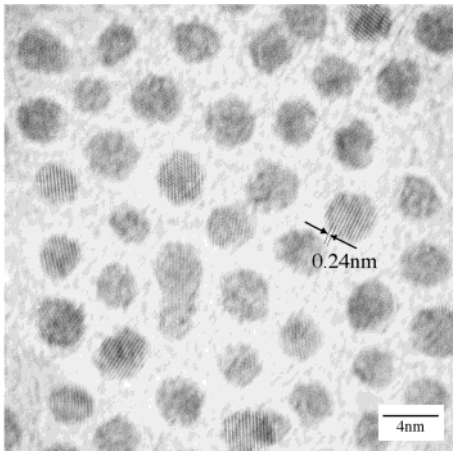

Figure 4. HRTEM image of DT−Au nanoparticles heat treated at 150 °C.

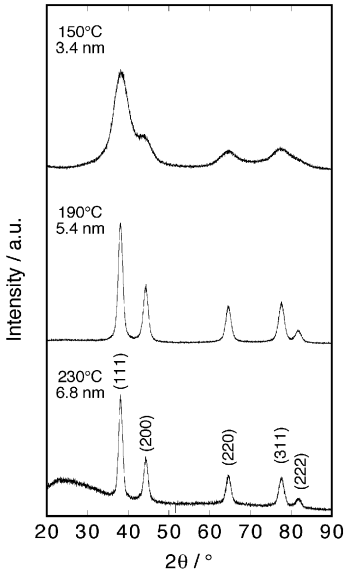

Figure 5. X-ray diffraction patterns of DT−Au nanoparticles after heat treatment at 150, 190, and 230 °C.

Formation of 2D Superlattices. The heat-treated Au nanoparticles form 2D superlattices with hexagonal packing covering an area of a few μm^2 on the flat carbon-coated (hydrophobic) copper grids during the toluene evaporation. (See Figure 2.) Then, we investigated the influence of substrate polarity on the formation of 2D superlattice of DT−Au nanoparticles by using hydrophilic mica and hydrophobic HOPG as substrates. Figure 6 shows the AFM images of 5.7-nm DT−Au nanoparticles on mica and HOPG prepared by evaporating a few drops of toluene solution containing DT−Au nanoparticles. The DT−Au nanoparticles aggregated on polar mica, whereas they formed 2D superlattice on the hydrophobic HOPG probably resulting from the hydrophobicity of the DT ligands. Thus, the similarity in polarities between the substrate (HOPG) and protective ligand (DT) is one of the necessary conditions in achieving 2D superlattice of nanoparticles. The thickness of the DT ligand layer estimated from an AFM image is 1.25 nm; this value is consistent with that estimated from a TEM image but is smaller than the DT ligand length (∼1.8 nm).[26]

Characterization of DT Ligands Before and After Heat Treatment. The atomic compositions of DT ligands on Au nanoparticles before and after heat treatment are estimated by elemental analysis. The results are summarized in Table 1, where the atomic ratios of carbon and hydrogen are normalized against

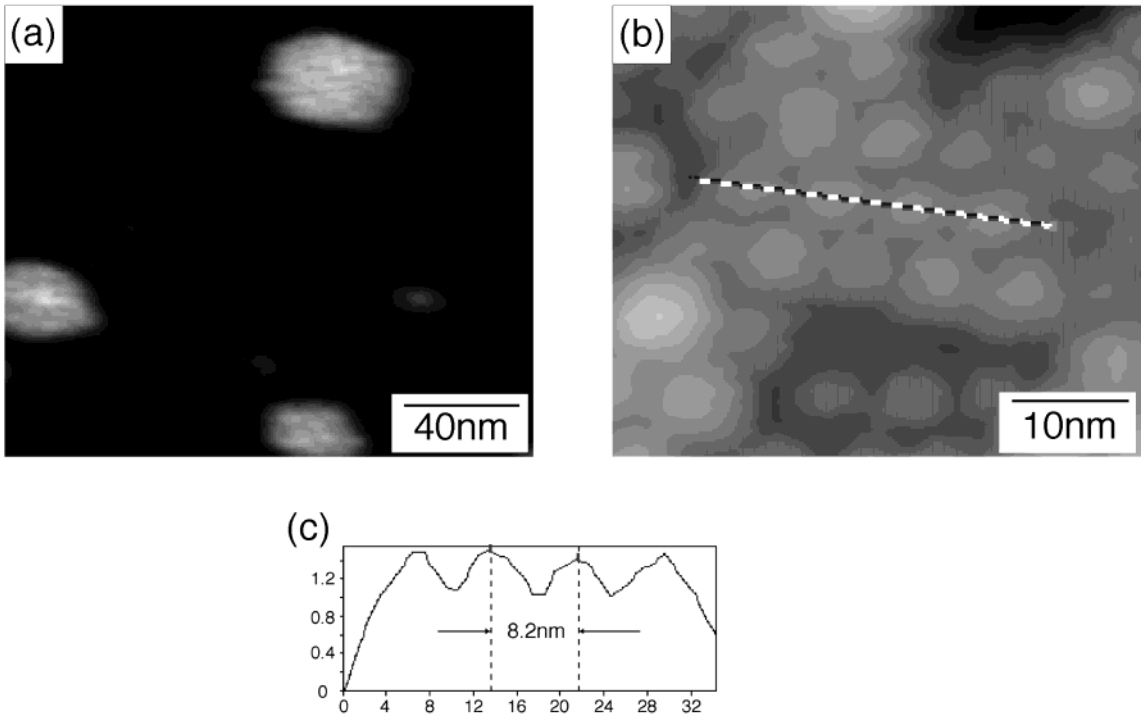

Figure 6. Tapping-mode AFM image of DT−Au nanoparticles after heat treatment at 200 °C on (a) mica and (b) HOPG and (c) cross-sectional profile along the line in b.

TABLE 1: Mean Diameters of DT−Au, Molecular Formulas of DT, Au Contents ([Au]), Ratio of Surface Atoms to All Atoms of Au Nanoparticles ($R_{Surf/All}$), and Number of Surface Au Atoms Occupied by One DT Ligand ($N_{Au(S)}$) in DT−Au Heat Treated under Various Temperatures

temp (°C)	mean diameter (nm)	molecular formula[a]	[Au] (wt %)[b]	$R_{surf/all}$ (%)	$N_{Au(S)}$
	1.5	$C_{12.6}H_{26.8}S$	71.9	62.6	1.7
150	3.4	$C_{11.8}H_{25.0}S$	79.7	39.2	1.6
190	5.4	$C_{10.0}H_{20.9}S$	93.3	25.9	3.2
230	6.8	$C_{9.6}H_{20.1}S$	94.7	20.6	3.1

[a] Estimated by elemental analysis. [b] Determined by TGA.

sulfur. The carbon number of the DT ligand decreased slightly upon increasing the heat-treatment temperature probably because of C−C bond cleavage, though the hydrocarbon chains retained the saturated structure as suggested by the constant C/H ratio of approximately $n/(2n + 1)$ for $S-(CH_2)_n-CH_3$.

The Au contents of DT−Au nanoparticles before and after heat treatment were estimated by TGA (Table 1). The Au content of as-prepared DT−Au nanoparticles is 71.9 wt %, compatible with the literature value.[14] This value indicates that approximately half of the surface Au atoms are bounds to DT ligands. By an increase in the heat-treatment temperature, the Au contents of DT−Au nanoparticles increased from 79.7 to 94.7 wt %. The ratio of surface atoms to all atoms of Au nanoparticles decreases to one-third of the original value (from 62.6% to 20.6%) with the heat-treatment temperature, whereas the number of surface Au atoms occupied by one DT ligand increased to less than twice the original value (from 1.7 to 3.1) upon increasing the heat-treatment temperature. Therefore, the desorption of DT ligands from the surface of Au nanoparticles may occur during the size evolution of Au nanoparticles.

FT-IR spectroscopy was applied to investigate the structure of DT ligands on the surface of Au nanoparticles. The peak positions for the symmetrical (d^+) and asymmetrical (d^-) stretching bands of methylene can be used as a sensitive indicator to estimate the degree of ordering of the alkyl chains.[27] For crystalline polyethylene (all-trans zigzag confirmation), d^+ and d^- appear at 2920 and 2850 cm^{-1}, respectively, and they shift to 2928 and 2856 cm^{-1}, respectively, for amorphous polyethylene (coexistence of trans and gauche conformations). The measured FT-IR spectra are shown in Figure 7. The methylene peaks corresponding to d^+ and d^- appeared at 2920 and 2850 cm^{-1}, respectively, for all of the samples irrespective of the heat treatment of DT−Au nanoparticles. These results indicate that the alkyl chains of the DT ligands on the Au surface have an all-trans conformation.

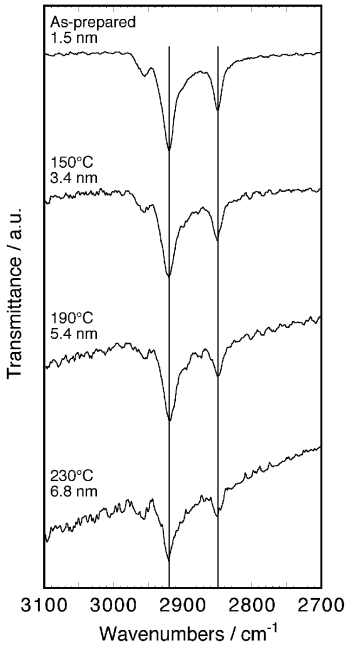

Figure 7. FT-IR spectra of DT−Au nanoparticles before and after heat treatment at various temperatures.

Taking such a stretched-chain structure of the DT ligands on the Au surface (1.8 nm in length) and the distance between Au

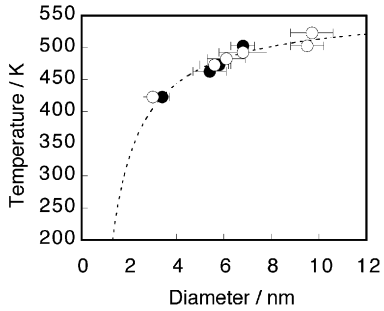

Figure 8. Relationship between the heat-treatment temperature and the size of DT−Au (●) and ODT−Au nanoparticles (○). The dotted line denotes a theoretically fit curve based on a melting curve of bulk Au.

nanoparticles estimated by TEM and AFM (1.25 nm) into consideration, we concluded that the DT ligands interpenetrate each other in 2D superlattices even after the heat-treatment process.[26]

Size-Evolution Mechanism of Au Nanoparticles. The precise size control established by the heat treatment may result from thermodynamic control (i.e., the smaller nanoparticle with the lower melting point grows uniformly until it becomes stable at the specific heat-treatment temperature). Such a size-evolution process should include sequential alkanethiol desorption from the particle surface, Au core coalescence accompanied by a rearrangement of Au atoms, and alkanethiol reprotection of the particle surface.[22] To understand the relationship between the mean diameters of alkanethiol-protected Au nanoparticles and the heat-treatment temperatures, we applied the thermodynamical model based on a melting curve of fine Au particles because the growth of nanoparticles should be induced by the melting of the particle surface. According to Buffat's thermodynamical model, the relationship between the mean diameters of naked metal particles and the melting temperatures is reported to be expressed by the following equation:[28−30]

$$\frac{T_d - T_\infty}{T_\infty} = -\frac{4}{\rho_s L d}\left[\gamma_s - \gamma_l\left(\frac{\rho_s}{\rho_l}\right)^{2/3}\right]$$

where d is the diameter of the particle, T_d and T_∞ are the melting temperatures for the particle and the bulk (1337 K),[31] respectively, ρ_s and ρ_l are the densities of the solid (19 000 kg/m^3) and liquid phases (17 280 kg/m^3), respectively, γ_s and γ_l are the surface energies of the solid (0.9 J/m^2) and liquid phases (0.74 J/m^2), respectively, and L is the heat of fusion (53 800 J/kg). (Values in parentheses are those reported for bulk Au.) Recently, Dick and co-workers[31] reported the size dependence of the melting temperature of silica-encapsulated gold nanoparticles determined by differential thermal analysis (DTA) coupled to thermal gravimetric analysis (TGA). They demonstrated that the above equation establishes the Au nanoparticles coated with silica when the surface-energy value of solid phase γ_s was modified to be 1 J/m^2. Such a modification is also expected to be effective for Au nanoparticles coated by another material, such as alkanethiol. When the values of $\gamma_s = 1$ J/m^2 and $T_\infty = 560$ K are adopted for the present heat-induced DT− and ODT−Au systems, experimental data fit the above equation well, as shown in Figure 8. El-Sayed et al.[32] have reported, on the basis of TEM observations, that the surface of Pt nanoparticles melts above 600 °C, which is much lower than the melting point of bulk Pt (1769 °C). A low T_∞ value of 560 K for Au nanoparticles compared to that of bulk Au (1337 K) may also be applicable in our case and may support a mechanism through the melting of the particle surface. The most plausible size-evolution mechanism for the present DT− and ODT−Au nanoparticles is proposed as follows: the surfaces of small DT− and ODT−Au nanoparticles melt by an increase in temperature, and the Au nanoparticles presumably uniformly coagulate to increase in size until they reach the specific temperature of 150−250 °C, where the particle surface becomes thermodynamically stable.[30]

Conclusions

We have demonstrated a new method for the heat-induced size evolution of small Au nanoparticles in the solid state. Once the small nanoparticles were prepared, we could obtain the monodispersed Au nanoparticles from 3.4 to 9.7 nm in size at heat-treatment temperature from 150 to 250 °C. The equation for the mean diameters and the heat-treatment temperatures based on the thermodynamic model proposed by Buffat was established for the present system after modifying the values of the surface energy of the solid phase and the melting temperature of Au. This suggests that the melting of the Au particle surface induced the particle growth. The interplane spacings of Au nanoparticles before and after heat treatment estimated by a HRTEM image and an XRD pattern are in good agreement with that of the bulk Au{111} plane (0.2355 nm). The heat-treated alkanethiol-protected Au nanoparticles form 2D superlattices with hexagonal packing on the flat hydrophobic substrates during the evaporation of toluene solution. The DT ligands are estimated to interpenetrate each other with an all-trans conformation in the 2D superlattices of DT−Au nanoparticles.

Our thermodynamic method to control the particle size is simple and quite useful in obtaining a large number of Au nanoparticle. The use of different ligands and/or additives to obtain larger Au particles for optical devices as well as the application of other metals is in progress. This technique will be applicable to the other ligand-protected metal or semiconductor nanoparticles.

Acknowledgment. This work was partially carried out in the Nanotechnology Glass Project as part of the Nanotechnology Materials Program supported by the New Energy and Industrial Technology Development Organization (NEDO) (M.M.) and was supported in part by a Grand-in-Aid for Scientific Research on Encouragement Research (A) (no. 13740392) from the Ministry of Education, Culture, Sports, Science and Technology, Japan (T.T.) and PRESTO, Japan Science and Technology corporation (T.T.).

References and Notes

(1) Freeman, R. G.; Grabar, K. C.; Allison, K. J.; Bright, R. M.; Davis, J. A.; Guthrie, A. P.; Hommer, M. B.; Jackson, M. A.; Smith, P. C.; Walter, D. G.; Natan, M. J. *Science (Washington, D.C.)* **1995**, *267*, 1629.

(2) Andres, R. P.; Bielefeld, J. D., Henderson, J. I.; Janes, D. B.; Kolagunta, V. R.; Kubiak, C. P.; Mahoney, W. J.; Osifchin, R. G. *Science (Washington, D.C.)* **1996**, *273*, 1690.

(3) Sun, S.; Murray, C. B.; Weller, D.; Folks, L.; Moser, A. *Science (Washington, D.C.)* **2000**, *287*, 1989.

(4) Black, C. T.; Murray, C. B.; Sandstrom, R. L.; Sun, S. *Science (Washington, D.C.)* **2000**, *290*, 1131.

(5) Tanahashi, S.; Manabe, Y.; Tohda, T.; Sasaki, S.; Nakamura, A. *J. Appl. Phys.* **1996**, *79*, 1244.

(6) Taleb, A.; Russier, V.; Courty, A.; Pileni, M. P. *Appl. Surf. Sci.* **2000**, *162−163*, 655.

(7) Teranishi, T.; Sugawara, A.; Shimizu, T.; Miyake, M., *J. Am. Chem. Soc.* **2002**, *124*, 4210.

(8) Bigioni, T. P.; Harrell, L. E.; Cullen, W. G.; Guthrie, D. E.; Whetten, R. L.; First, P. N. *Eur. Phys. J. D* **1999**, *6*, 355.

(9) Andres, R. P.; Bein, T.; Dorogi, M.; Feng, S.; Henderson, J. I.; Kubiak, C. P.; Mahoney, W.; Osifchin, R. G.; Reifenberger, R. *Science (Washington, D.C.)* **1996**, *272*, 1323.

(10) Thomas, P. J.; Kulkarni, G. U.; Rao, C. N. R. *Chem. Phys. Lett.* **2000**, *321*, 163.

(11) Schmid, G.; Bäumle, M.; Beyer, N. *Angew. Chem., Int. Ed.* **2000**, *39*, 181.

(12) Teranishi, T.; Haga, M.; Shiozawa, Y.; Miyake, M. *J. Am. Chem. Soc.* **2000**, *122*, 4237.

(13) Galletto, P.; Brevet, P. F.; Girault, H. H.; Antoine, R.; Broyer, M. *J. Phys. Chem. B* **1999**, *103*, 8706.

(14) Green, M.; O'Brien, P. *Chem. Commun.* **2000**, 183.

(15) Teranishi, T.; Kiyokawa, I.; Miyake, M. *Adv. Mater.* **1998**, *10*, 596.

(16) Teranishi, T.; Hosoe, M.; Miyake, M. *Adv. Mater.* **1997**, *9*, 65.

(17) Teranishi, T.; Miyake, M. *Chem. Mater.* **1998**, *10*, 594.

(18) Teranishi, T.; Hosoe, M.; Tanaka, T.; Miyake, M. *J. Phys. Chem. B* **1999**, *103*, 3818.

(19) Brust, M.; Walker, M.; Bethell, D.; Schiffrin, D. J.; Whyman, R. *J. Chem. Soc., Chem. Commun.* **1994**, 801.

(20) Brust, M.; Fink, J.; Bethell, D.; Schiffrin, D. J.; Kiely, C. *J. Chem. Soc., Chem. Commun.* **1995**, 1655.

(21) Leff, D. V.; Ohara, P. C.; Heath, J. R.; Gelbart, W. M. *J. Phys. Chem.* **1995**, *99*, 7036.

(22) Maye, M. M.; Zheng, W. X.; Leibowitz, F. L.; Ly, N. K.; Zhong, C. J. *Langmuir* **2000**, *16*, 490.

(23) Maye, M. M.; Zhong, C. J. *J. Mater. Chem.* **2000**, *10*, 1895.

(24) Teranishi, T.; Hasegawa, S.; Shimizu, T.; Miyake, M. *Adv. Mater.* **2001**, *13*, 1699.

(25) Alvarez, M. M.; Khoury, J. T.; Schaaff, T. G.; Shafigullin, M. N.; Vezmar, I.; Whetten, R. L. *J. Phys. Chem. B* **1997**, *101*, 3706.

(26) Giersig, M.; Mulvaney, P. *Langmuir* **1993**, *9*, 3408.

(27) Hostetler, M. I.; Stokes, J. J.; Murray, R. W. *Langmuir* **1996**, *12*, 3604.

(28) Buffat, Ph.; Borel, J. P. *Phys. Rev. A.* **1976**, *13*, 2287.

(29) Borel, J. P. *Surf. Sci.* **1981**, *106*, 1.

(30) Lewis, L. J.; Jensen, P.; Barrat, J.-L. *Phys. Rev. B.* **1997**, *56*, 2248.

(31) Dick, K.; Dhanasekaran, T.; Zhang, Z.; Meisei, D. *J. Am. Chem. Soc.* **2002**, *124*, 2312.

(32) Wang, Z. L.; Petroski, J. M.; Green, T. C.; El-Sayed, M. A. *J. Phys. Chem. B* **1998**, *102*, 6145.